RAA 2021 Vol. **21** No. **3**, 51(14pp) doi: 10.1088/1674-4527/21/3/51

http://www.raa-journal.org *http://iopscience.iop.org/raa*

***R**esearch in*
***A**stronomy and*
***A**strophysics*

On the radial velocity calibrations in the LAMOST medium-resolution spectroscopic survey of nebulae

Juan-Juan Ren[1,3], Hong Wu[2,3], Chao-Jian Wu[2,3], Wei Zhang[2,3], Jian-Jun Chen[2,3], Chih-Hao Hsia[4], Fan Yang[2,3], Chao Liu[1,3,5], Jian-Rong Shi[2,3,5], Yu-Zhong Wu[2,3], Hui Zhu[3], Bin Li[6,7], Zhong-Rui Bai[2,3], Hao Tian[1,3] and Yong-Hui Hou[8,9]

[1] CAS Key Laboratory of Space Astronomy and Technology, National Astronomical Observatories, Chinese Academy of Sciences, Beijing 100101, China; *jjren@nao.cas.cn*
[2] CAS Key Laboratory of Optical Astronomy, National Astronomical Observatories, Chinese Academy of Sciences, Beijing 100101, China
[3] National Astronomical Observatories, Chinese Academy of Sciences, Beijing 100101, China
[4] State Key Laboratory of Lunar and Planetary Sciences, Macau University of Science and Technology, Taipa, Macau, China
[5] University of Chinese Academy of Sciences, Beijing 100049, China
[6] Purple Mountain Observatory, Chinese Academy of Sciences, Nanjing 210008, China
[7] University of Science and Technology of China, Hefei 230026, China
[8] Nanjing Institute of Astronomical Optics & Technology, National Astronomical Observatories, Chinese Academy of Sciences, Nanjing 210042, China
[9] School of Astronomy and Space Science, University of Chinese Academy of Sciences, Beijing 100049, China

Received 2020 March 31; accepted 2020 August 10

Abstract Accurate radial velocity determinations of optical emission lines (i.e., [N II] $\lambda\lambda$ 6548, 6584, Hα and [S II] $\lambda\lambda$ 6717, 6731) are very important for investigating the kinematic and dynamic properties of nebulae. The second stage survey program of Large sky Area Multi-Object fiber Spectroscopic Telescope (LAMOST) has started a sub-survey of nebulae (MRS-N) which will spectroscopically observe the optical emission lines of a large sample of nebulae near the Galactic plane. Until now, 15 MRS-N plates have been observed from September 2017 to June 2019. Based on fitting the sky emission lines in the red band spectra of MRS-N, we investigate the precision of wavelength calibration and find there are systematic deviations of radial velocities (RVs) from $\sim$0.2 to 4 $\mathrm{km\,s^{-1}}$ for different plates. Especially for the plates obtained in March 2018, the systematic deviations of RVs can be as large as $\sim$4 $\mathrm{km\,s^{-1}}$, which then go down to $\sim$0.2 – 0.5 $\mathrm{km\,s^{-1}}$at the end of 2018 and January 2019. An RV calibration function is proposed for these MRS-N plates, which can simultaneously and successfully calibrate the systematic deviations and improve the precision of RVs.

Key words: ISM: general — ISM: kinematics and dynamics — technique: spectroscopic — technique: radial velocities

1 INTRODUCTION

Nebulae are interstellar clouds consisting of dust, hydrogen, helium and other ionized gases. Among the various types of nebulae, emission nebulae are clouds of interstellar ionized gases and dust that emit light in various wavelengths. There are different kinds of emission nebulae, including H II regions, planetary nebulae (PNe), supernova remnants (SNRs; Woltjer 1972) and so on. Different types of emission nebulae have various different formation mechanisms, thus they can be used to study many aspects of astronomical sciences from star formation to the evolution of the Milky Way. H II regions can be applied as probes of the composition of the interstellar medium in a galaxy, and their emission-line spectrum can be utilized to determine the gas-phase abundance of several elements (Shaver et al. 1983; Esteban et al. 2019). Due to the bright emission lines of PNe, they can be relied on as tracers of galaxy kinematics (Merrett et al. 2006), and as potential tracers of the chemical evolution of the Milky Way and other galaxies (Cavichia et al. 2017; Kwitter et al. 2012). SNRs can provide insights into

the mechanisms of supernova explosions, and probe the immediate surroundings of supernovae. SNRs are also fundamentally related to the star-forming process in a galaxy, and can also give us a picture of the on-going massive star formation rate (Kopsacheili et al. 2020).

Optical spectroscopic observations of emission nebulae can provide important information on nebulae, especially the Hα, Hβ, [N II] $\lambda\lambda$ 6548, 6584, [S II] $\lambda\lambda$ 6717, 6731, [O II] $\lambda\lambda$ 3726, 3729 and [O III] $\lambda\lambda$ 4959, 5007. These optical emission lines can be utilized to investigate the kinematic and dynamic properties of nebulae (Damiani et al. 2016). Furthermore, the optical line intensity ratio [S II] λ 6717/[S II] λ 6731 is electron density sensitive (Osterbrock & Ferland 2006), the Hα/[S II] $\lambda\lambda$ 6717,6731 ratio can be used to distinguish shocked nebulae from photoionized nebulae (Alvarez & Hoare 2005) and the Hα/[N II] ratio is a widely employed tool for investigating nitrogen-to-hydrogen abundance variations among SNRs (Fesen et al. 1985). Combining the emission line ratios with the kinematics of ionized gas can be used to characterize and identify the nature of nebulae. Thus it is very important to obtain a complete sampling of the optical line emissions in various nebulae. A lot of optical spectrophotometric observations have been carried out for emission nebulae. However, most of them are only dedicated to some special nebulae (Fesen et al. 1985; Blair et al. 1991; Gerardy & Fesen 2007; Chen et al. 2017), and thus a spectroscopic survey that includes a large sample of nebulae near the Galactic plane is still lacking, especially for cases with large spatial size.

The Large sky Area Multi-Object fiber Spectroscopic Telescope (LAMOST) is a quasi-meridian reflecting Schmidt telescope, which has a $\sim$4 meter effective aperture and a field of view of 5° in diameter (Wang et al. 1996; Su & Cui 2004; Cui et al. 2012; Zhao et al. 2012). As a dedicated spectroscopic survey telescope, LAMOST can acquire optical spectra with 4000 fibers during one single exposure. Since September 2012, LAMOST has been carrying out the first five-year Regular Surveys, i.e. the first stage survey program of LAMOST (hereafter LAMOST I). The LAMOST I Regular Surveys mainly consist of two components (Zhao et al. 2012): the LAMOST Extra-Galactic Survey of Galaxies (LEGAS) that aims to study the large scale structure of the Universe; and the LAMOST Experiment for Galactic Understanding and Exploration (LEGUE; Deng et al. 2012) with the goal of obtaining millions of stellar spectra to study the structure and evolution of the Milky Way. The LAMOST I spectra cover the entire optical wavelength range ($\simeq$ 3700 – 9000 Å), with a resolving power $R \sim 1800$ (Luo et al. 2012, 2015).

Since September 2017, the second stage survey program of LAMOST (hereafter LAMOST II) was initiated. Besides continuing the low-resolution spectroscopic observations, LAMOST II began the medium-resolution spectroscopic survey (MRS; Liu et al. 2020). In every lunar month, half of the nights (i.e., the dark/gray nights, from the 23rd to the 6th on the lunar calendar) have been devoted to continuing the previous low-resolution spectroscopic surveys, while the remaining half of the nights (i.e., the bright/gray nights, from the 7th to the 22nd on the lunar calendar) have been assigned for the MRS. LAMOST II MRS spectra have a medium-resolution of $R \sim 7500$, and cover the wavelength ranges of 4950 – 5350 Å in blue channel and 6300 – 6800 Å in red channel (Wu et al. 2020a). The main scientific aims of LAMOST II MRS include the time-domain (TD) and non-time-domain (NT) sciences. Hence the MRS survey can be broken down into a few different sub-surveys: the Kepler region survey (MRS-K), the TESS follow-up survey (MRS-T), the Star forming region survey (MRS-S), the Binary survey (MRS-B), the Galactic Nebulae survey (MRS-N), the Galactic archaeology survey (MRS-G) and Open cluster survey (MRS-O). Among them, MRS-K, MRS-T, MRS-B and some fields of MRS-S are assigned as the TD survey, while the MRS-G, MRS-N, MRS-O and part of the MRS-S are operated as the NT survey (Liu et al. 2020).

The large field of view (5°), relatively higher resolution (7500) and dedicated wavelength coverage (6300 – 6800 Å, thus covering the emission lines Hα, [N II] $\lambda\lambda$ 6548, 6584 and [S II] $\lambda\lambda$ 6717, 6731), make LAMOST II MRS an ideal spectroscopic survey to sample the optical emission lines of Galactic nebulae (Wu et al. 2020b) in unprecedented detail. To better investigate the kinematic properties of nebulae, one of the most important things is to obtain better wavelength calibration thus improving the radial velocity (RV) determination of nebula emission lines.

In this paper, we investigate the wavelength calibration and finally propose a method to improve the precision of the RV determinations in the LAMOST II MRS-N survey. In Section 2, we describe the observation and data reduction of the LAMOST II MRS-N survey. In Section 3 we present the method, and Section 4 provides a discussion. Finally Section 5 gives a summary.

2 LAMOST II MRS-N OBSERVATION AND DATA REDUCTION

2.1 Observation

The LAMOST II MRS-N survey aims at obtaining the medium-resolution spectra of a large sample of Galactic nebulae including the H II regions, PNe, SNRs and Herbig-Haro objects (Wu et al. 2020b). The MRS-N survey contains two components: (1) obtaining the optical spectra of emission lines of a large sample of Galactic nebulae in the Galactic plane ($40° < l < 218°$,

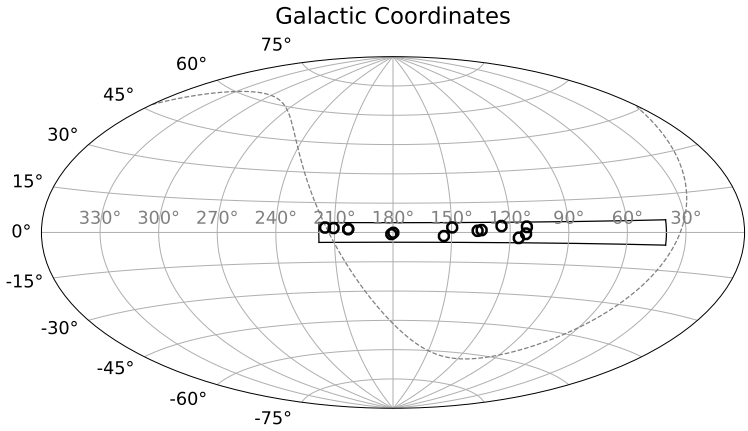

Fig. 1 The Galactic coordinates of the 15 MRS-N plates (*black open circles*). The *black rectangle* signifies the survey region of MRS-N, i.e., $40° < l < 218°$ and $-5° < b < 5°$.

$-5° < b < 5°$, ~ 1700 deg^2 totally), with every field having only one observation; (2) acquiring the optical spectra of four specially selected nebulae: Westerhout 5 (H II regions), Rosette Nebula + NGC 2264 (H II region), Cygnus Loop (SNRs) and Simeis 147 (SNRs), each one with more than 10 observations during the five-year regular survey. As the moonlight has a serious influence on the nebula observation, which makes the sky subtraction very difficult for nebula spectra, the MRS-N observations only were carried out during moonless gray/bright nights. The LAMOST II MRS-N survey was initiated in September 2017. The first year of the survey was a pilot survey, and the first regular survey started since September 2018.

Until June 2019, 15 MRS-N plates had been observed. Table 1 lists detailed information on these 15 MRS-N plates. Figure 1 shows their Galactic distribution. From Table 1 and Figure 1, we can see that most of the observed MRS-N plates are concentrated near the Galactic anti-center, with the Galactic longitude in the range 110°–215° and the Galactic latitude between $-2.7°$ and $3.2°$. Most of the MRS-N plates have exposure time 900 s $\times$ 3, which is relatively shorter than the exposure time of normal star observations (1200 s $\times$ 3) of MRS. There are two reasons: (1) the very limited observation time for nebula observation, which should be carried out during moonless gray/bright nights; (2) another reason should be that the 900 s $\times$ 3 exposure is already enough to obtain good quality emission line spectra of nebulae.

2.2 Data Reduction

As the MRS-N observations and scientific goals are very different from other normal MRS surveys, there will be a new dedicated data reduction pipeline for the MRS-N survey (Wu et al. 2021c, in preparation). The LAMOST MRS raw spectra are processed with the LAMOST two-dimensional (2D) pipeline (Luo et al. 2015), including the dark and bias subtraction, cosmic ray removal, one-dimensional (1D) spectral extraction and wavelength calibration. The MRS wavelength calibration procedures are similar to those for the LAMOST low-resolution spectral reduction pipeline (as described in Luo et al. 2015) by using arc lines. We need to note that Sc lamps were utilized before May 2018, and then Th-Ar lamps were installed instead. After the extraction of arc lamp spectra, the centroids of the arc lines are measured, which will be used to fit a Legendre polynomial (fifth-order in the blue channel, and sixth-order in the red) as a function to describe the relationship between wavelengths and pixels. Then the wavelength will be calibrated to vacuum, and also corrected to the heliocentric frame (Luo et al. 2015). Usually about 42 Th-Ar arc lines or 13 Sc arc lines (only for the data obtained before May 2018) are referenced for the wavelength calibration of MRS spectra (see Fig. 2 for an example of Sc and Th-Ar arc lamp spectra). For different fibers, the number of arc lines considered will be a little different due to their possibly slightly different wavelength coverage. The MRS-N pipeline began with the 1D sub-spectra (output from the LAMOST 2D pipeline), which are wavelength calibrated, but without sky subtraction and flux calibration.

Then the MRS-N pipeline will merge the sub-spectra (usually three sub-exposures for each plate), re-calibrate the wavelength (the work we will investigate and propose in this paper), do the sky subtraction (Zhang et al. 2021, in preparation), fit the emission lines in the red band (i.e., Hα, [N II] $\lambda\lambda$ 6548, 6584 and [S II] $\lambda\lambda$ 6717, 6731) and finally publish the value-added catalog for the MRS-N survey, which includes the emission line RVs, line widths and line intensity ratios (as presented in Ren et al. 2018b). About 50%–80% of the [N II] and [S II] has spectral signal to noise ratio (S/N) > 10, and 80%–95% of Hα can have S/N > 10,

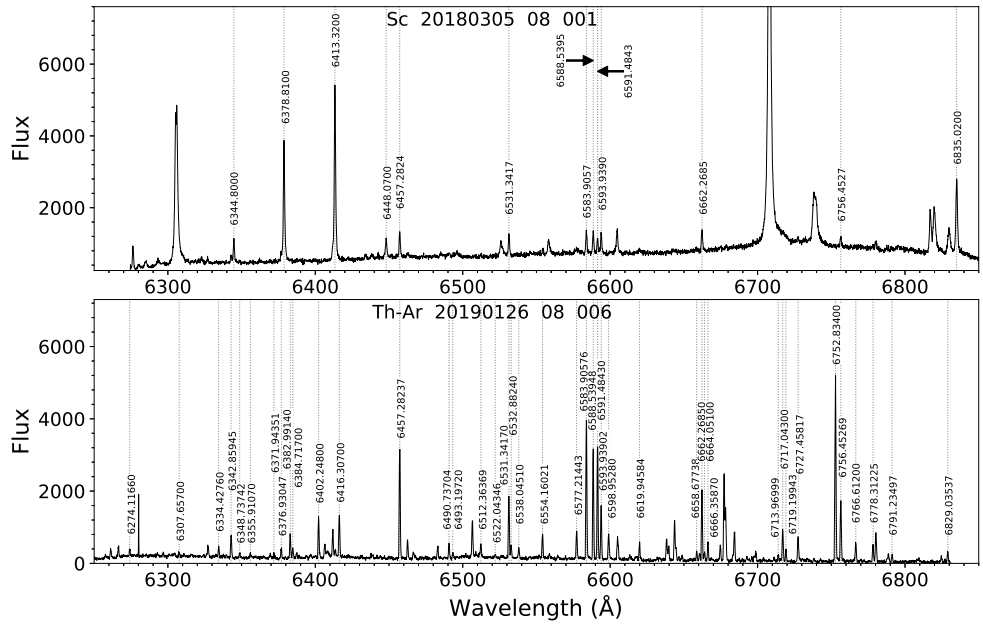

Fig. 2 An example Sc (*upper panel*) and Th-Ar (*lower panel*) arc lamp spectrum in red band. The *vertical gray dotted lines* mark the arc lines referenced for MRS wavelength calibration.

Table 1 The 15 Plates Observed by LAMOST II MRS-N in the Pilot and the First Year Regular Survey (from September 2017 to June 2019)

ObsDate	Plate	Center Star	RA (°)	Dec (°)	l (°)	b (°)	Seeing (arcsec)	Exp (s)
20180305	HD474690101	HD47469	99.7966	9.64596	202.956762	1.691792	5.6	900 s × 3
20180305	HD474690801	HD47469	99.7966	9.64596	202.956762	1.691792	4.8	900 s × 3
20181018	NT054437N290059N01	HIP27088	86.1573	29.0166	179.818302	−0.142857	2.4	1200 s × 3
20181118	NT070341S003325N01	HIP34039	105.9240	−0.556953	214.826342	2.472767	3.4	900 s × 3
20181128	NT230608N631246N01	HIP114070	346.5370	63.2128	111.391030	2.724941	2.9	900 s × 3
20181128	NT235302N592517N01	HIP117772	358.2600	59.4216	115.557042	−2.611379	2.9	900 s × 3
20181129	NT010552N655815N01	HIP115228	16.4707	65.9711	124.403798	3.140640	3.7	900 s × 3
20181129	NT232020N601629N01	HIP5147	350.0870	60.2748	111.866024	−0.625150	3.6	900 s × 3
20181216	NT065450N031415N01	HIP33227	103.7110	3.23735	210.437214	2.232564	5.0	900 s × 3
20181228	NT023239N614403N01	HD15557	38.1664	61.7342	134.613668	1.180085	5.3	900 s × 3
20190124	NT024709N603414N01	HD17086	41.7903	60.5708	136.683682	0.826460	2.7	900 s × 3, 1200 s × 2
20190125	NT041422N543127N01	HIP19774	63.5933	54.5242	149.660595	2.546033	2.8	900 s × 3
20190125	NT041453N482433N01	HIP19812	63.7244	48.4093	153.939273	−1.824453	2.9	900 s × 3
20190126	NT054421N274353N01	HD38084	86.0882	27.7315	180.881876	−0.866799	3.5	900 s × 3
20190126	NT054421N274353N02	HD38084	86.0882	27.7315	180.881876	−0.866799	3.7	900 s × 2

depending on the sky regions observed (Wu et al. 2021, in preparation).

Here we need to note that the LAMOST II MRS spectra have wavelength coverage: 4950 – 5350 Å in blue channel and 6300 – 6800 Å in red channel. The blue spectra of MRS cannot cover the important nebula emission features in blue band (i.e., Hβ, [O II] $\lambda\lambda$ 3726,3729). Only [O III] $\lambda\lambda$ 4959,5007 is available in the MRS blue spectra, but it is usually not as strong and visible as the emission features in the red band (Hα, [N II] $\lambda\lambda$ 6548, 6584, and [S II] $\lambda\lambda$ 6717, 6731). Thus, finally the MRS-N data reduction will only focus on the red band, and the final value-added MRS-N catalog only provides information determined from the red spectra. Figure 3 features an example spectrum of MRS-N in red band.

Table 2 The Obvious Seven Single Sky Emission Lines in the Red Band Spectra of MRS-N

N	Name	Wavelength (air) (Å)	Wavelength (vacuum) (Å)
1	λ6287	6287.434	6289.1730
2	λ6300	6300.304	6302.0464
3	λ6363	6363.780	6365.5395
4	λ6498	6498.729	6500.5248
5	λ6533	6533.044	6534.8490
6	λ6544	6544.022	6545.8299
7	λ6553	6553.617	6555.4275

3 METHOD

Accurate RV determinations of emission lines are very important for studying the kinematic and dynamic properties of nebulae. While for the MRS observations,

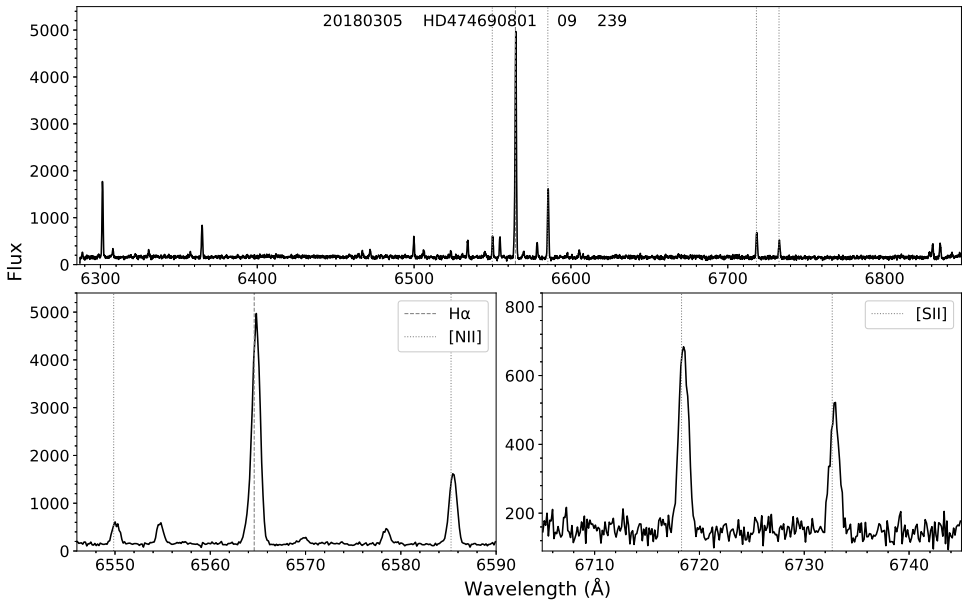

Fig. 3 An example MRS spectrum of nebulae in red band (spectrum ID "20180305-HD474690801-09-239"). The bottom panels showcase the zoomed regions near the main emission features Hα, [N II] $\lambda\lambda$ 6548, 6584 and [S II] $\lambda\lambda$ 6717, 6731.

the arcs (Th-Ar) referenced for wavelength calibration are obtained before or after the normal observations (i.e., not simultaneously). Thus the wavelength calibration from arcs may incorporate some uncertainties for RV determinations, due to direction change of the telescope or environment variation (such as temperature, pressure) in the spectrograph room. To acquire accurate RV measurements, it is necessary to do a calibration. Unlike the RV calibrations of stars which can be obtained by relying on RV standard stars (Liu et al. 2019; Wang et al. 2019), the main targets in MRS-N are nebula features, not stars. Thus, a new method should be developed to investigate the wavelength calibration precision and propose new RV calibration ways to improve the RV precision in MRS-N survey data.

For the LAMOST low-resolution spectral reduction, some strong sky emission lines were utilized during the wavelength calibration procedure. But for the MRS spectra, the sky emission lines were not used in the 2D data reduction pipeline. As we mentioned in Section 1, the MRS observations were carried out during the bright/gray nights (from the 7th to the 22nd on the lunar calendar) every month. That means the moonlight background is very bright during the MRS observations for most times, and the corresponding sky emission lines have very low S/N, and thus are not available for wavelength calibration. But for our MRS-N survey, the observations are scheduled only during the moonless bright/gray nights, thus the sky emission lines still have good quality, and can be applied to help us improve the MRS-N wavelength calibration.

In the MRS-N 1D wavelength calibrated spectra without sky subtraction, there are several sky emission lines as visible in Figure 3. There are 13 obvious sky emission lines in the red band (Osterbrock et al. 1996), among which seven are single lines as listed in Table 2 and six are blended lines as presented in Table 3. Figure 4 displays an example MRS-N spectrum showing these sky emission lines. Initially we hope to use all these sky emission lines (seven single + six blended lines) to calibrate RVs. By carefully investigating the blending situation and line profiles of the blended lines, we find it is hard to differentiate the multiple peaks of the blended lines, thus it is impossible to obtain accurate line centers even by multi-Gaussian fitting under our relatively low resolution ($\sim$ 7500) spectra. Much higher resolution ($\sim$ 30 000) spectra are needed to differentiate the multiple peaks of the blended lines well (Osterbrock et al. 1996). If we apply single Gaussian fitting to these blended lines, the fitted line centers may have relatively large uncertainties due to their blending features. Hence finally we exclude these six blended lines from our following analysis, and only use the seven single lines. These sky emission lines cover a relatively large wavelength range (6290 – 6560 Å) of the MRS-N red spectra (see Fig. 4), and their intrinsic wavelengths are already well-known and fixed (see Table 2), thus they are ideal tools to investigate the precision of wavelength calibration of MRS in real time. Furthermore, the sky emission lines are obtained at the same time as the nebula emission lines, so most importantly they can provide a simultaneous RV calibration and finally help us improve the precision of RV determinations of MRS-N.

The Gaussian fitting method is widely utilized for measuring the stellar RVs based on SDSS

Table 3 Similar to Table 2, But for Six Blended Sky Emission Lines

N	Name	Wavelength (air) (Å)	Wavelength (vacuum) (Å)
1	λ6306	[6306.869, 6306.981]	[6308.6132, 6308.7252]
2	λ6329	[6329.747, 6329.933]	[6331.4974, 6331.6834]
3	λ6356	[6356.167, 6356.441]	[6357.9244, 6358.1985]
4	λ6604	[6603.990, 6604.279]	[6605.8140, 6606.1031]
5	λ6829	[6827.459, 6828.469, 6829.491, 6829.564, 6829.922]	[6829.3432, 6830.3534, 6831.3757, 6831.4487, 6831.8068]
6	λ6834	[6834.008, 6834.433]	[6835.8939, 6836.3190]

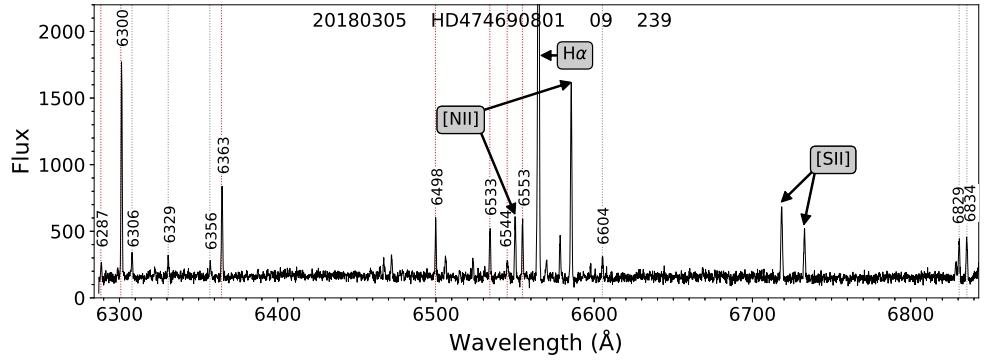

Fig. 4 An example MRS-N spectrum showing the sky emission lines in red band (spectrum ID "20180305-HD474690801-09-239"). The *red dotted lines* mark single lines listed in Table 2, while the *gray dotted lines* signify the blended lines presented in Table 3.

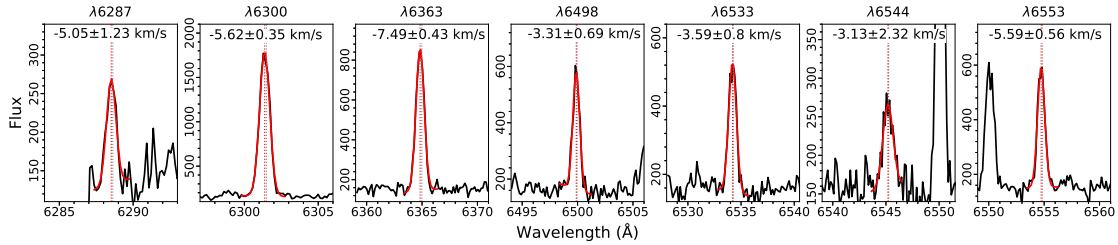

Fig. 5 An example of single-Gaussian fitting of the sky emission lines (spectrum ID "20180305-HD474690801-09-239") for seven single lines. The *red curves* trace the Gaussian fitted results, and the *red dotted lines* signify the fitted centers. The *gray dotted lines* are the true line centers as listed in Table 2.

(Rebassa-Mansergas et al. 2016) or LAMOST spectra (Ren et al. 2018a). Usually a second-order polynomial plus a single-Gaussian line profile is used to fit a single line (such as Hα emission line), while a second-order polynomial plus a double/triple-Gaussian line profile with fixed separation is used to fit double/triple lines (like Na I $\lambda\lambda$ 8183.27, 8194.81 or Ca II absorption triplet at 8498.02, 8542.09 and 8662.14 Å), as described in Rebassa-Mansergas et al. (2007, 2017) and Ren et al. (2013, 2014). Here we adopt a similar method, i.e., a second-order polynomial plus a single-Gaussian line profile is applied to fit the seven single sky emission lines in Table 2. Figure 5 shows an example of the Gaussian fitting results of one nebula spectrum.

Table 4 lists the fitting results for every spectrum of the 15 MRS-N plates. For those strong sky emission lines like λ6300 and λ6363 (as displayed in Figs. 4 and 5), the fitting error is only $\lesssim 0.4-0.5\,\mathrm{km\,s^{-1}}$; for those not so strong lines like λ6498, λ6533 and λ6553, the fitting error is $\lesssim 0.7-1.0\,\mathrm{km\,s^{-1}}$; even for those relatively weak emission lines (i.e., λ6287 and λ6544), the fitting error is mostly $\lesssim 1.6-2\,\mathrm{km\,s^{-1}}$, all of which demonstrate the good quality of sky emission lines, thus affirming them to be the best tools to investigate and improve the precision of RV determinations of nebula emission lines. From Figure 5, we can see that there is obvious systematic deviation around $4\,\mathrm{km\,s^{-1}}$ for the RV of this spectrum.

To investigate the situation of the whole plate, we obtain the mean and standard deviation of the fitted sky RVs for every MRS-N plate (see Table 5), by Gaussian-fitting of the histogram distribution of sky RVs. Figure 6 features the histogram distribution of the fitted RVs for the seven single sky emission lines for plate "20180305-HD474690801". For those relatively strong sky emission lines (i.e., λ6300, λ6363, λ6498, λ6533, λ6553), the standard deviation is lower ($\sim 1.2-2.0\,\mathrm{km\,s^{-1}}$); while for

Table 4 The Fitted RVs of Seven Single Sky Emission Lines for the Spectra from the 15 MRS-N Plates

SpecID	RV_{6287} ($km\,s^{-1}$)	RV_{6300} ($km\,s^{-1}$)	RV_{6363} ($km\,s^{-1}$)	RV_{6498} ($km\,s^{-1}$)	RV_{6533} ($km\,s^{-1}$)	RV_{6544} ($km\,s^{-1}$)	RV_{6553} ($km\,s^{-1}$)
20190126-NT054421N274353N01-02-120	−4.68±1.33	−1.77±0.46	−0.19±0.46	−0.66±0.58	−1.26±1.05	−3.87±1.64	0.07±0.98
20190126-NT054421N274353N01-02-121	−4.96±1.65	−1.64±0.48	−0.28±0.56	−2.36±1.02	−1.85±1.16	−6.26±2.04	−2.95±0.84
20190126-NT054421N274353N01-02-122	−4.37±1.85	−0.10±0.30	1.56±0.40	0.27±0.82	1.16±0.65	4.75±0.71	0.70±1.44
20190126-NT054421N274353N01-02-123	−5.68±1.97	−1.46±0.54	0.71±0.75	−0.69±0.73	−1.25±0.78	−1.84±1.40	−2.58±0.93
20190126-NT054421N274353N01-02-124	0.93±1.79	−0.06±0.46	0.29±0.61	0.14±0.50	−1.18±0.89	−6.52±2.39	−2.22±0.84
20190126-NT054421N274353N01-02-125	−6.53±1.66	−0.80±0.35	−1.51±0.63	1.72±0.72	0.78±1.16	−2.02±2.51	−2.11±0.71
20190126-NT054421N274353N01-02-126	−5.26±1.11	0.68±0.30	0.51±0.30	−0.95±0.81	−0.44±1.19	−0.05±2.63	−0.69±0.74
20190126-NT054421N274353N01-02-127	0.15±2.80	0.81±0.41	2.42±0.63	−1.52±0.67	−1.65±0.62	−0.42±2.01	0.18±0.52
20190126-NT054421N274353N01-02-128	−7.03±1.40	1.18±0.27	0.93±0.53	0.60±0.84	0.30±0.96	1.76±1.24	−1.02±0.99
20190126-NT054421N274353N01-02-129	2.54±2.58	1.28±0.42	1.37±0.56	−1.28±0.73	−1.86±1.30	−1.85±2.38	−0.43±0.91
20190126-NT054421N274353N01-02-130	−1.95±1.17	0.27±0.67	0.81±0.52	−0.08±0.98	−0.75±0.79	−6.32±2.51	−1.29±1.15

'−' marks cases where the RVs are unavailable. Here just list part of the table, the complete table can be found in `http://www.raa-journal.org/docs/Supp/ms4700tab4.csv`.

those relatively weak lines (such as λ6287, λ6544), the standard deviation is a little large ($\sim 2.4-3.4\,km\,s^{-1}$), which can be easily explained as the weak lines having low spectral quality that thus can transfer relatively large fitted uncertainties. From Figure 6 and Table 5, we can clearly see the systematic deviation of wavelength calibration for almost the whole plate, thus it is very necessary to calibrate these systematic deviations to obtain accurate RVs of nebula emission lines.

Then by using the fitted line center of these seven single sky emission lines (as displayed in Fig. 6 and Table 5), a second-order polynomial was used to do the fit. We also try the third- and fourth-order polynomial fit, but they exhibit obvious over-fitting, thus we suggest that the second-order polynomial fitting is the best choice. Furthermore, as we mentioned before, the seven single sky emission lines we used cover the wavelength range: 6290 – 6560 Å, which should be enough to calibrate the RVs of Hα and [N II] $\lambda\lambda$ 6548, 6584 emission lines of nebulae. However, another important emission line, i.e., [S II] $\lambda\lambda$ 6717, 6731 is located far from this range. We then extrapolate the RV calibration to 6731 Å by applying a constraint that the RV calibrations at 6731 Å and 6548 Å are similar. Thus at least we can correct the systematic deviations at $\sim$ 6731 Å. Finally the RV calibration function is fitted by using the seven single sky emission lines and the value extrapolated at 6731 Å. Figure 7 shows an example of the fitted RV calibration function (the red curve).

After the calibration, the sky RVs can be as accurate as $0\,km\,s^{-1}$(which is the true RVs of sky emission lines) with a standard deviation of $0.5770\,km\,s^{-1}$, but before the calibration, the sky RVs have a systemic uncertainty as large as $-3.9192\,km\,s^{-1}$ with a standard deviation $0.7500\,km\,s^{-1}$, for plate "20180305-HD474690801" as demonstrated in Figure 7. Furthermore, when fitting the RV calibration function, we suggest making an RV error cut of $3\,km\,s^{-1}$ for the sky emission lines. When we also try an RV error cut of $1.5\,km\,s^{-1}$, the fitted RV calibration function did not show a large difference, thus the RV error cut of $3\,km\,s^{-1}$ is suggested to be used.

4 DISCUSSION

We applied the method described in the previous section for all the 15 MRS-N plates. Table 6 lists the fitted parameters of the RV calibration function ($f(x) = a\,x^2 + b\,x + c$, where x is the wavelength in unit of μm). We need to note that for the 10 plates observed in March/December 2018 and January 2019, the seven single sky emission lines (the black points plotted in Fig. 7) are already very good for providing accurate RV calibration.

But for the five plates observed in November 2018, we need to remove two sky lines, λ6287 and λ6300, at the blue end (for the one plate in October 2018, only remove one sky line λ6287), as the histogram distributions of the line centers of λ6287 and λ6300 are not single Gaussian symmetric or even multi-peaked (which is the situation shown in Fig. 8). In order to investigate the multi-peak features of these sky RVs of the plates on November 2018, we present the coordinate distribution of seven sky RVs for plate "20181118-NT070341S003325N01" in Figure 9. For reference, the rightmost panel illustrates the spatial distribution of the 16 spectrographs. We can see that for the sky RVs from λ6287 and λ6300, almost half of the spectrographs focused around another peak (see the red dots in the left two panels). By carefully checking the spectra obtained in the "green" and "red" spectrographs (the blue and red dots in the left two panels respectively), we can clearly see a large shift in the emission lines λ6287 and λ6300. That means, for these five MRS-N plates observed in November 2018, there are large systematic deviations near 6300 Å for almost half of the spectrographs, which should be due to the bad wavelength calibration in this region. As we can see in the bottom panel of Figure 2, there are only two very weak arc lines near 6300 Å which thus may lead to bad wavelength calibration near this region when these two lines are too weak and have bad quality.

In December 2018, the systematic deviation near 6300 Å has disappeared. Figure 10 shows the coordinate distribution of sky RVs for one plate observed in December

Table 5 The Gaussian-fitted Mean and Standard Deviation of the Histogram Distribution of Sky RVs for 15 MRS-N Plates

ObsDate	plateID	μ_{6287} ($\mathrm{km\,s^{-1}}$)	μ_{6300} ($\mathrm{km\,s^{-1}}$)	μ_{6363} ($\mathrm{km\,s^{-1}}$)	μ_{6498} ($\mathrm{km\,s^{-1}}$)	μ_{6533} ($\mathrm{km\,s^{-1}}$)	μ_{6544} ($\mathrm{km\,s^{-1}}$)	μ_{6553} ($\mathrm{km\,s^{-1}}$)
20180305	HD474690101	−4.16±3.23	−4.56±1.71	−5.76±1.40	−3.24±1.34	−3.50±1.35	−3.50±2.71	−3.99±1.23
20180305	HD474690801	−4.18±3.33	−4.38±1.81	−5.60±1.40	−3.08±1.31	−3.36±1.29	−3.44±2.43	−3.76±1.16
20181018	NT054437N290059N01	–	−7.67±2.54	−4.52±1.46	−1.76±1.32	−1.96±1.39	−1.73±2.39	−2.19±1.21
20181118	NT070341S003325N01	–	–	0.82±1.33	0.71±1.21	0.21±1.27	0.34±1.70	−0.03±1.16
20181128	NT230608N631246N01	–	–	−0.41±2.26	−0.35±2.26	−0.25±2.19	0.02±4.01	−0.52±2.06
20181128	NT235302N592517N01	–	–	−0.06±1.97	−0.18±2.07	−0.05±2.02	0.14±3.27	−0.30±1.92
20181129	NT010552N655815N01	–	–	0.80±1.81	0.01±2.27	0.11±2.27	0.55±3.88	0.20±2.16
20181129	NT232020N601629N01	–	–	0.45±2.03	0.02±2.20	0.16±2.17	0.33±3.46	0.09±2.01
20181216	NT065450N031415N01	−0.62±2.69	0.51±1.24	0.63±1.44	0.29±1.30	0.08±1.39	0.08±2.65	−0.28±1.28
20181228	NT023239N614403N01	−0.61±2.93	0.42±1.91	0.67±1.97	0.63±1.76	0.17±1.75	0.30±2.79	−0.02±1.65
20190124	NT024709N603414N01	−1.36±3.37	−0.40±1.58	−0.32±1.51	−0.58±1.61	−0.70±1.73	−0.31±3.35	−0.95±1.57
20190125	NT041422N543127N01	−0.51±3.53	0.42±1.48	0.44±1.44	−0.06±1.84	−0.42±1.90	−0.03±3.87	−0.52±1.86
20190125	NT041453N482433N01	−0.62±2.77	0.34±1.24	0.46±1.31	0.03±1.47	−0.32±1.41	−0.17±2.46	−0.42±1.35
20190126	NT054421N274353N01	−0.55±3.06	0.46±1.25	0.46±1.41	−0.15±1.48	−0.38±1.52	−0.21±2.97	−0.56±1.42
20190126	NT054421N274353N02	−0.61±3.27	0.44±1.31	0.37±1.67	−0.21±1.55	−0.43±1.65	−0.33±3.23	−0.68±1.48

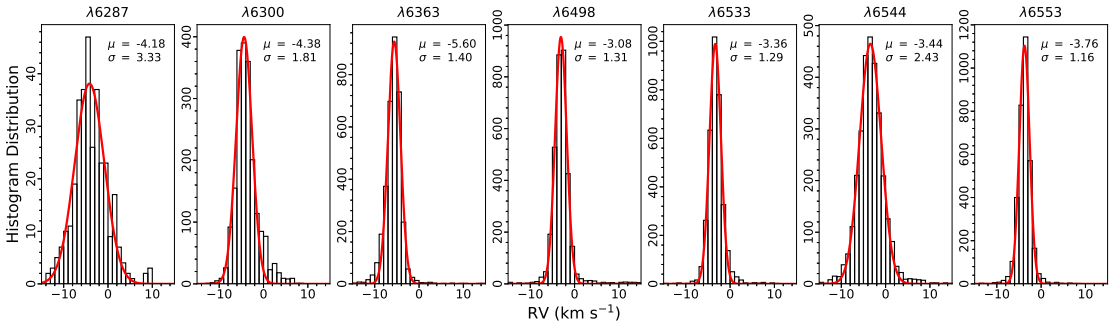

Fig. 6 The histogram distribution of the RVs of seven single sky emission lines for MRS-N plate "20180305-HD474690801". The *red curves* are the Gaussian fitting results of the histogram distributions, and the μ and σ marked in each panel are the line center and standard deviation of the fitting respectively.

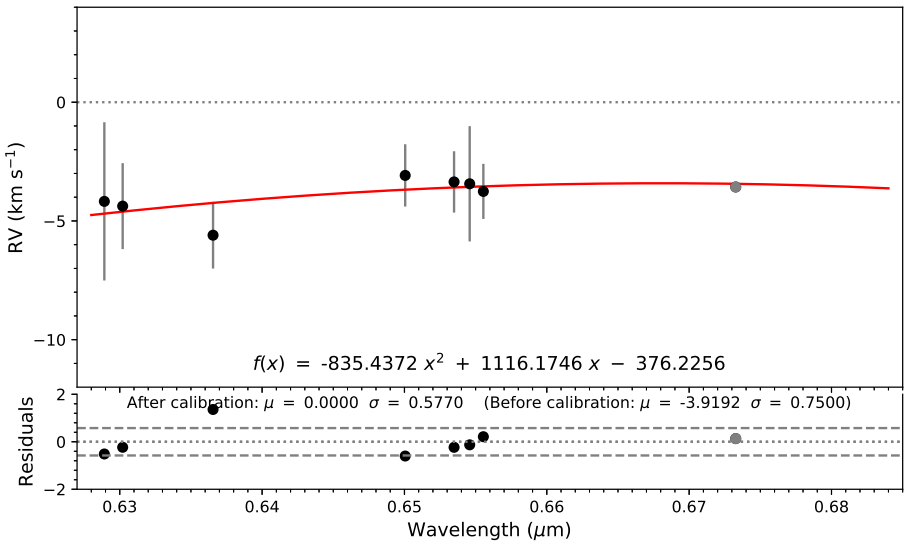

Fig. 7 An example of the fitted RV calibration function (plateID "20180305-HD474690801"). The seven *black dots* represent the fitted mean RVs of the seven single sky emission lines presented in Table 6, and the *rightmost gray dot* corresponds to the extrapolated value at 6731 Å. The *red curve* plots the fitted RVs calibration function for this plate. The bottom panel features the residuals, where the *gray dotted horizontal line* signifies the mean value of the residuals and the *gray dashed lines* mark the 1σ standard deviations.

Table 6 The parameters of the RV calibration function ($f(x) = ax^2 + bx + c$, where x is the wavelength in unit of μm) for the 15 MRS-N plates. The mean and standard deviation of sky RVs before and after the calibration are also listed. The last column "Flag" marks the sky lines (i.e., the line number as shown in the first column of Table 2) used to fit the RVs calibration function.

ObsDate	plateID	a	b	c	$\mu_{\rm before}$ ($\rm km\,s^{-1}$)	$\sigma_{\rm before}$ ($\rm km\,s^{-1}$)	$\mu_{\rm after}$ ($\rm km\,s^{-1}$)	$\sigma_{\rm after}$ ($\rm km\,s^{-1}$)	Flag
20180305	HD474690101	−738.7490	989.4288	−334.8446	−4.0503	0.7568	0.0000	0.6041	1, 2, 3, 4, 5, 6, 7
20180305	HD474690801	−835.4372	1116.1746	−376.2256	−3.9192	0.7500	0.0000	0.5770	1, 2, 3, 4, 5, 6, 7
20181018	NT054437N290059N01	−5739.5264	7601.2190	−2518.0593	−3.1091	2.0729	0.0000	0.4036	2, 3, 4, 5, 6, 7
20181118	NT070341S003325N01	742.0199	−991.7874	331.5405	0.3730	0.3019	0.0000	0.1868	3, 4, 5, 6, 7
20181128	NT230608N631246N01	−135.3334	182.7665	−61.9151	−0.2862	0.1686	0.0000	0.1570	3, 4, 5, 6, 7
20181128	NT235302N592517N01	118.2756	−154.3496	50.2610	−0.0816	0.1334	0.0000	0.1319	3, 4, 5, 6, 7
20181129	NT010552N655815N01	1153.0985	−1519.0363	500.4621	0.3454	0.2697	0.0000	0.1834	3, 4, 5, 6, 7
20181129	NT232020N601629N01	571.4184	−753.3775	248.4534	0.2159	0.1444	0.0000	0.1032	3, 4, 5, 6, 7
20181216	NT065450N031415N01	−425.1480	547.7008	−176.2284	0.0767	0.3814	0.0000	0.3664	1, 2, 3, 4, 5, 6, 7
20181228	NT023239N614403N01	−663.7146	864.6065	−281.2221	0.2142	0.3820	0.0000	0.3537	1, 2, 3, 4, 5, 6, 7
20190124	NT024709N603414N01	−311.3390	408.5562	−134.5974	−0.6480	0.3334	0.0000	0.3211	1, 2, 3, 4, 5, 6, 7
20190125	NT041422N543127N01	69.5751	−99.9254	35.4064	−0.1149	0.3594	0.0000	0.3327	1, 2, 3, 4, 5, 6, 7
20190125	NT041453N482433N01	−158.2488	197.4298	−61.5766	−0.1214	0.3502	0.0000	0.3300	1, 2, 3, 4, 5, 6, 7
20190126	NT054421N274353N01	58.2406	−88.3461	32.6192	−0.1598	0.3824	0.0000	0.3375	1, 2, 3, 4, 5, 6, 7
20190126	NT054421N274353N02	68.5436	−103.3951	37.9632	−0.2390	0.3970	0.0000	0.3409	1, 2, 3, 4, 5, 6, 7

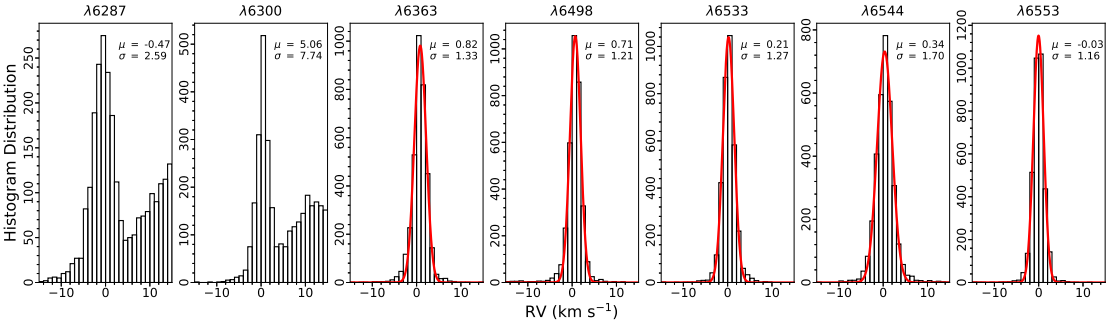

Fig. 8 Same as Fig. 6, but for plate "20181118-NT070341S003325N01", for which the distribution of sky RVs at λ6287 and λ6300 has multiple peaks, and thus are not used for fitting the RV calibration function of this plate.

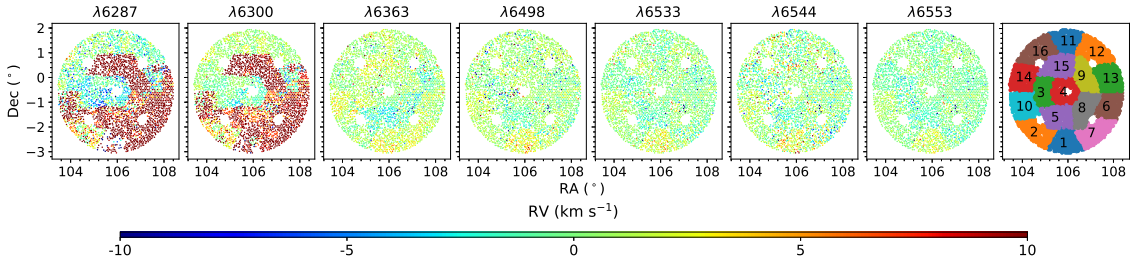

Fig. 9 The coordinate (RA, Dec) distribution of the RVs of seven sky emission lines for plate "20181118-NT070341S003325N01". The color bar shows the value of sky RVs. For reference, the rightmost panel illustrates the distribution of the 16 spectrographs.

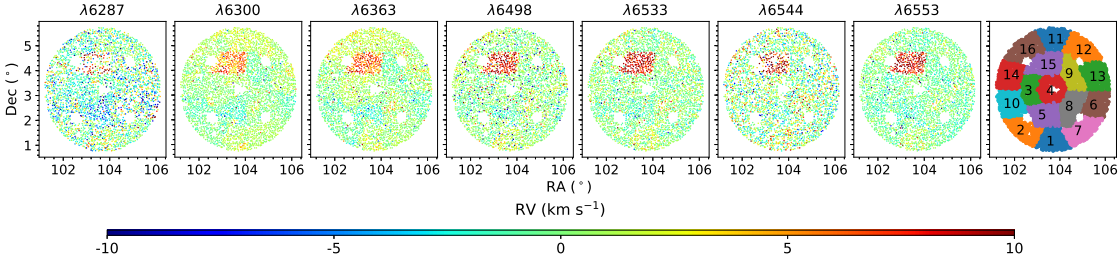

Fig. 10 Same as Fig. 9, but for plate "20181216-NT065450N031415N01".

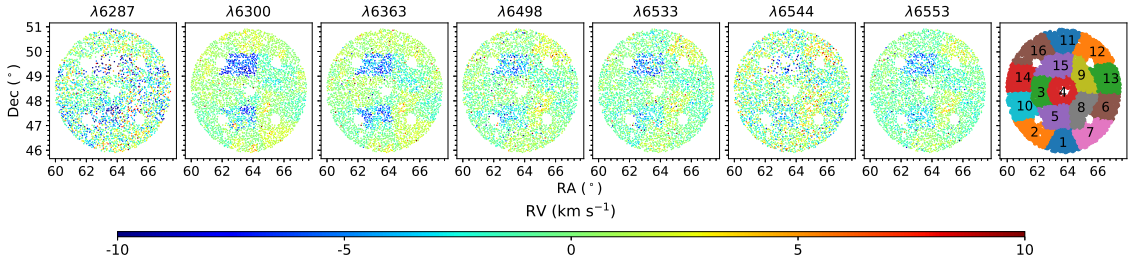

Fig. 11 Same as Fig. 9, but for plate "20190125-NT041453N482433N01".

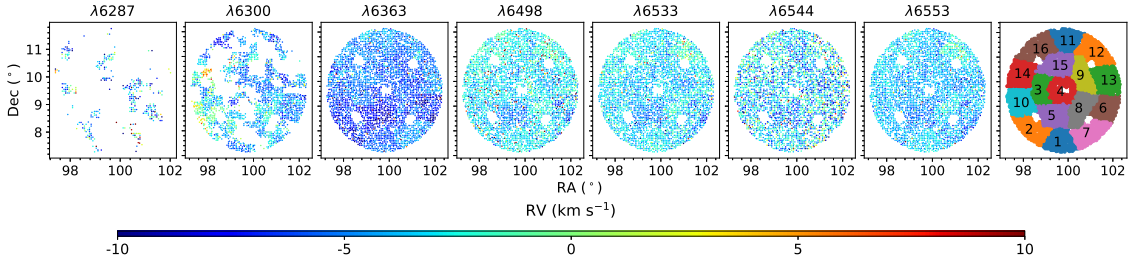

Fig. 12 Same as Fig. 9, but for plate "20180305-HD474690801".

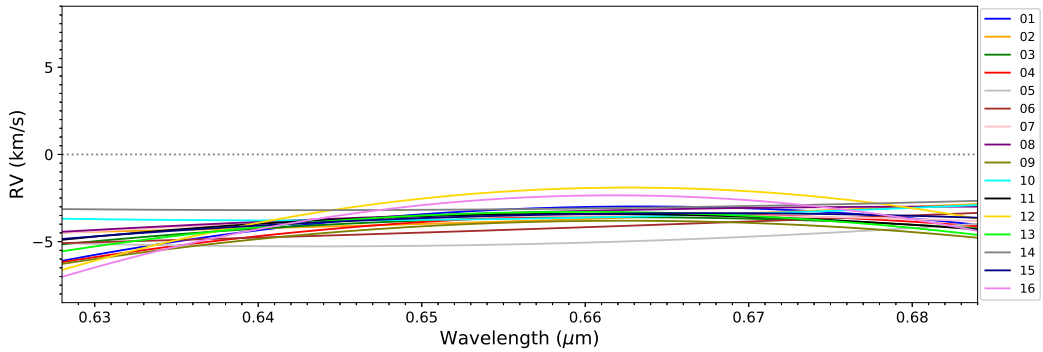

Fig. 13 The fitted RV calibration function of 16 spectrographs from plate "20180305-HD474690801". The colors represent different spectrographs.

2018, i.e., "20181216-NT065450N031415N01". Although the problem of multiple peaks has disappeared near 6300 Å, there is another obvious problem: one of the spectrographs, i.e., spectrograph 15, has a large ($\gtrsim 5\,\mathrm{km\,s^{-1}}$) systematic difference from the other spectrographs. Then by checking the five plates observed in January 2019, we find this effect still exists. Figure 11 shows the situation of one plate obtained in January 2019, i.e. plate "20190125-NT041453N482433N01", from which we can see that the systematic difference of the spectrograph becomes negative by comparing with Figure 10, and another spectrograph (ID: 5) has the same situation. This can be explained due to the spectrograph drift for these two spectrographs (i.e., 15 and 5).

While for the two plates observed in March 2018, the situation is very different from the above plates (see Fig. 12), which is totally dominated by the systematic deviation ($\sim 4\,\mathrm{km\,s^{-1}}$, which can also be seen from Table 6) of the whole spectra for the whole plate. Moreover, those bluer than 6363 Å are even worse than those redder than 6363 Å, which can also be seen from Figures 7 and 6. This can be easily explained, as in March 2018, the arc lamp for MRS used was the Sc lamp, which only has a very limited number of arc lines (as shown in the top panel of Fig. 2), thus affecting the wavelength calibration and finally resulting in the large systematic deviations of the two MRS-N plates in March 2018.

From Tables 5 – 6 and above discussions, we can see that for the two MRS-N plates in March 2018 and one plate in October, there are large systematic deviations around $2 \sim 4\,\mathrm{km\,s^{-1}}$ for the whole plate, which can be roughly eliminated after our calibration presented in Table 6. While for the five plates observed in November 2018, two plates in December 2018 and five plates in January 2019, the systematic deviations of the whole plates are around $0.2 \sim 0.5\,\mathrm{km\,s^{-1}}$, which can also be roughly calibrated after applying our calibrations in Table 6. The decrease of the systematic deviations of the whole plates from early

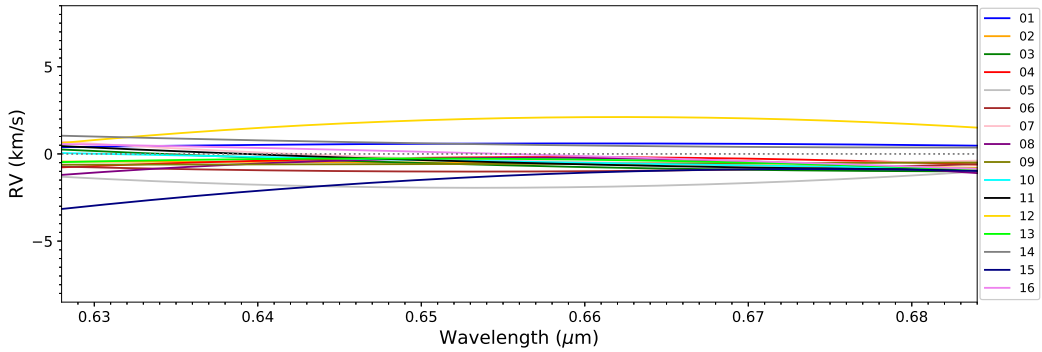

Fig. 14 Same as Fig. 13, but for the plate "20190126-NT054421N274353N01".

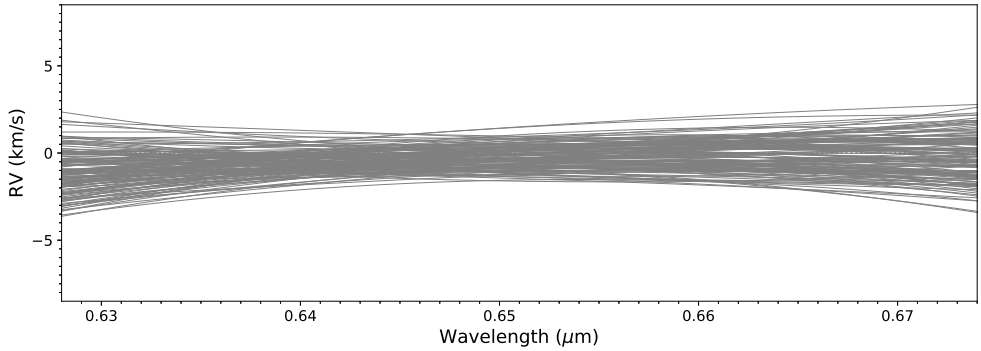

Fig. 15 The fitted RV calibration function of all the spectra in one spectrograph (ID: 04) of plate "20190126-NT054421N274353N02".

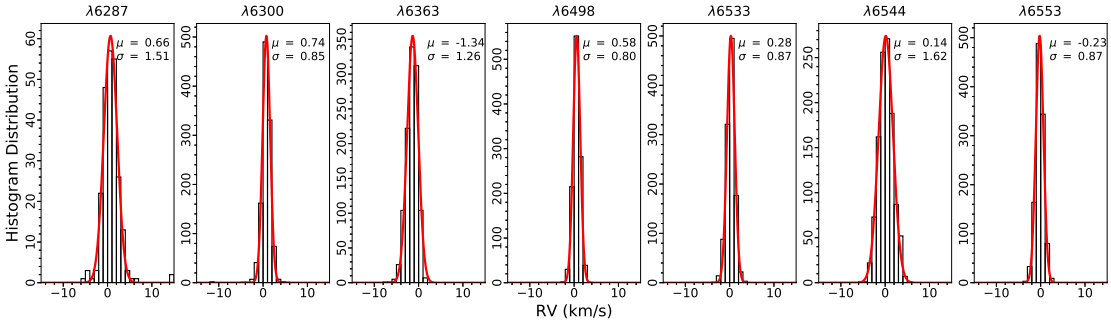

Fig. 16 The histogram distribution of sky RVs after applying the RV calibration function in Table 8 (for plate "20180305-HD474690801").

2018 to late 2018 indicates that the wavelength calibration has been improved at least since November 2018. The improvement of MRS wavelength calibration from early 2018 to 2019 was mainly due to the updates of arc lamps: (1) In early 2018, the arc lamp used by MRS was Sc which only had a very limited number of available arc lines as we mentioned before, and the Sc lamp had serious systematic deviation of about $4 \sim 5\,\mathrm{km\,s^{-1}}$; (2) From May 2018, MRS began to rely on a Th-Ar lamp, but only 10 Th-Ar lamps were employed initially. Due to the long optical path and large focal plane of LAMOST, only utilizing 10 Th-Ar lamps was not enough to get high enough brightness and uniform distribution of illumination, which thus may affect the wavelength calibration. (3) At the end of 2018 and beginning of 2019, the number of Th-Ar lamps was increased from 10 to 20, which enhanced the brightness and uniformity of illumination, thus improving the wavelength calibration of MRS in 2019.

Although the wavelength calibration of MRS was improved at the end of 2018 and beginning of 2019, there are still some problems such as the spectrograph drift effect as mentioned previously (see Figs. 10–11). Thus, we also investigate the distribution of sky RVs for different spectrographs of the same plate. Figures A.1 and A.2 feature the histogram distribution of sky RVs and the fitted calibration function for two different spectrographs (i.e., spectrograph ID 04 and 08 of plate "20180305-HD474690801") on one plate. We can

Table 7 The parameters of the RV calibration function ($f(x) = ax^2 + bx + c$, where x is the wavelength in unit of μm) for the 16 spectrographs of 15 MRS-N plates.

Spectrograph ID	a	b	c	$\mu_{\rm before}$	$\sigma_{\rm before}$ ($\rm km\,s^{-1}$)	$\mu_{\rm after}$ ($\rm km\,s^{-1}$)	$\sigma_{\rm after}$ ($\rm km\,s^{-1}$)	Flag ($\rm km\,s^{-1}$)
20180305-HD474690101-01	−2456.7311	3270.5386	−1091.5202	−4.0119	1.1733	0.0000	0.5054	2, 3, 4, 5, 6, 7
20180305-HD474690101-02	−32.0486	77.3790	−40.8026	−4.0333	1.3238	0.0000	1.2405	2, 3, 4, 5, 6, 7
20180305-HD474690101-03	−1273.8805	1693.2619	−566.2647	−4.0538	0.6751	0.0000	0.4312	2, 3, 4, 5, 6, 7
20180305-HD474690101-04	−2166.7051	2870.7681	−954.6600	−4.6506	1.0882	0.0000	0.5559	1, 2, 3, 4, 5, 6, 7
20180305-HD474690101-05	1220.1428	−1580.3003	506.3375	−5.1127	1.1884	0.0000	1.1602	1, 2, 3, 4, 5, 6, 7
20180305-HD474690101-06	−566.5774	764.2089	−261.8449	−4.6631	0.9684	0.0000	0.8718	1, 2, 3, 4, 5, 6, 7
20180305-HD474690101-07	−1200.3801	1568.7877	−516.6348	−4.2810	0.5673	0.0000	0.5080	2, 3, 4, 5, 6, 7
20180305-HD474690101-08	240.1561	−287.3387	81.5520	−3.7576	1.0876	0.0000	1.0308	1, 2, 3, 4, 5, 6, 7
20180305-HD474690101-09	−587.3293	795.5451	−273.2511	−4.4821	0.8819	0.0000	0.7382	1, 2, 3, 4, 5, 6, 7
20180305-HD474690101-10	261.0949	−327.5368	98.7891	−3.7470	1.1004	0.0000	1.0875	2, 3, 4, 5, 6, 7
20180305-HD474690101-11	−1329.2261	1757.0361	−584.1550	−3.8879	0.5716	0.0000	0.3699	2, 3, 4, 5, 6, 7
20180305-HD474690101-12	−3540.2103	4693.6972	−1557.8253	−3.2085	1.3672	0.0000	0.3912	2, 3, 4, 5, 6, 7
20180305-HD474690101-13	−2064.6018	2722.2270	−900.7025	−3.8765	0.6929	0.0000	0.3311	2, 3, 4, 5, 6, 7
20180305-HD474690101-14	797.1745	−1044.9741	339.1450	−3.1014	0.9919	0.0000	0.9674	1, 2, 3, 4, 5, 6, 7
20180305-HD474690101-15	−309.2930	426.8453	−150.7229	−4.0662	0.7151	0.0000	0.6162	1, 2, 3, 4, 5, 6, 7
20180305-HD474690101-16	−4376.8213	5796.9788	−1921.7888	−3.6397	1.6030	0.0000	0.3867	2, 3, 4, 5, 6, 7
20180305-HD474690801-01	−2484.6439	3296.8155	−1096.5995	−3.8144	1.1004	0.0000	0.5585	2, 3, 4, 5, 6, 7
20180305-HD474690801-02	214.8080	−252.7951	69.5716	−4.0027	1.2683	0.0000	1.2134	1, 2, 3, 4, 5, 6, 7
20180305-HD474690801-03	−1340.9390	1775.6265	−591.4048	−4.0029	0.6132	0.0000	0.3912	2, 3, 4, 5, 6, 7
20180305-HD474690801-04	−1995.4816	2654.7405	−886.3688	−4.4149	1.1345	0.0000	0.5393	1, 2, 3, 4, 5, 6, 7

The mean and standard deviation of sky RVs before and after the calibration are also listed. The last column "Flag" marks the sky lines (i.e., the line number as shown in the first column of Table 2) used to fit the RV calibration function. The complete table can be found online in `http://www.raa-journal.org/docs/Supp/ms4700tab7.csv`.

Table 8 The parameters of the RV calibration function ($f(x) = ax^2 + bx + c$, where x is the wavelength in unit of μm) for every spectrum of the 15 MRS-N plates.

SpecID	a	b	c	$\mu_{\rm before}$ ($\rm km\,s^{-1}$)	$\sigma_{\rm before}$ ($\rm km\,s^{-1}$)	$\mu_{\rm after}$ ($\rm km\,s^{-1}$)	$\sigma_{\rm after}$ ($\rm km\,s^{-1}$)	Flag
20180305-HD474690101-01-007	−2648.5858	3452.2209	−1127.7720	−3.2969	1.2592	0.0000	1.1414	2, 3, 4, 5, 6, 7
20180305-HD474690101-01-008	−1607.8895	2142.9616	−715.9577	−2.6088	0.9337	0.0000	0.5929	2, 3, 4, 5, 6, 7
20180305-HD474690101-01-013	−1700.5175	2243.1382	−742.9757	−3.6736	0.9163	0.0000	0.7608	2, 3, 4, 5, 6, 7
20180305-HD474690101-01-016	−2461.9163	3284.7194	−1097.8069	−3.2688	1.3906	0.0000	0.7883	2, 3, 4, 5, 6, 7
20180305-HD474690101-01-017	−1924.3222	2584.4421	−869.8695	−3.2884	1.4040	0.0000	0.8745	2, 3, 4, 5, 6, 7
20180305-HD474690101-01-018	−3428.3998	4525.5355	−1496.2565	−3.6981	1.2518	0.0000	0.6652	2, 3, 4, 5, 6, 7
20180305-HD474690101-01-019	−1635.4571	2246.1514	−771.9583	−3.1524	1.8688	0.0000	1.0396	2, 3, 4, 5, 6, 7
20180305-HD474690101-01-020	−3727.5943	4977.1512	−1662.7970	−3.1154	1.9093	0.0000	0.6945	2, 3, 4, 5, 6, 7
20180305-HD474690101-01-022	−4079.3504	5453.0305	−1823.4475	−3.1107	2.1314	0.0000	0.6809	2, 3, 4, 5, 6, 7
20180305-HD474690101-01-024	−4138.4885	5465.6417	−1808.0232	−4.5188	1.4273	0.0000	0.5717	2, 3, 4, 5, 6, 7
20180305-HD474690101-01-025	−4198.3574	5553.6022	−1839.4810	−4.1017	1.4810	0.0000	0.4275	2, 3, 4, 5, 6, 7
20180305-HD474690101-01-027	−1727.4051	2253.5927	−739.1745	−4.4544	0.9819	0.0000	0.9172	2, 3, 4, 5, 6, 7

The last column "Flag" marks the sky lines (i.e., the line number as shown in the first column of Table 2) we used to fit the RV calibration function. The complete table can be found online in `http://www.raa-journal.org/docs/Supp/ms4700tab8.csv`.

see a clear difference between the systematic deviation (around $0.5\,\rm km\,s^{-1}$) of the these two spectrographs. Figure 13 plots the RV calibration function of all the 16 spectrographs of plate "20180305-HD474690801". There is a systematic deviation of about $3\sim4\,\rm km\,s^{-1}$ between these 16 spectrographs, which implies the RV calibration should be different for different spectrographs even in the same plate. Even for those plates in January 2019, the systematic deviations between different spectrographs still exist, as apparent in Figure 14 and Figure 11. Table 7 lists the fitted calibration function for the 16 spectrographs of the 15 MRS-N plates.

Although most of the sky RVs from one plate or spectrograph are focused near a peak (as depicted in Figs. 6, A.1 and A.2), there are still some fibers with sky RVs a little far from the peak value. To obtain higher precision of RV determinations, it is also necessary to provide an RV calibration function for every nebula spectrum, not only the whole plate or spectrograph. Figure 15 showcases an example of the fitted RV calibration functions of all the spectra in one spectrograph of one plate. We can see that even in one spectrograph, the fitted calibration function of each spectrum is still a little different. Thus it should be better to do the calibration for each spectrum. Table 8 lists the parameters of the fitted RV calibration function for every spectrum. For those without sky RVs available due to their low spectral quality or shortage of data, the RV calibration function of very nearby spectra can be applied instead. Figure 16 displays an example (for plate "20180305-HD474690801") of the

histogram distribution of sky RVs after applying the RV calibration function provided in Table 8. We can see that systematic deviation as large as $4\,\mathrm{km\,s^{-1}}$ has disappeared, especially for those sky lines near 6550 Å which harbor important nebula emission features (i.e., Hα, [N II] $\lambda\lambda$ 6548, 6584).

The future MRS-N pipeline (Wu et al. 2021c, in preparation) will adopt the method developed here to investigate the precision of wavelength calibration of MRS-N nebula spectra in real time, and fit an RV calibration function for every nebula spectrum by using sky emission lines to finally improve the precision of nebula RVs. Furthermore, this method is also valuable for other sub-surveys of MRS if they have some plates fortunately with available strong sky emission lines.

5 SUMMARY

The LAMOST II MRS survey has initiated a sub-survey of nebulae, i.e., MRS-N survey, since September 2017. The MRS-N survey will monitor a large sample of nebula emission line features, mainly including [N II] $\lambda\lambda$ 6548, 6584, Hα and [S II] $\lambda\lambda$ 6717, 6731. Before studying the kinematic and dynamic properties of nebulae, it is important to investigate the precision of the wavelength calibration of nebula spectra, and finally calibrate RVs of nebula emission lines.

We propose a method to investigate the precision of wavelength calibration of MRS-N, by considering sky emission lines in the red spectra of MRS. We find that the RVs of the 15 observed MRS-N plates have systematic deviations from $\sim$0.2 to $4\,\mathrm{km\,s^{-1}}$for different plates obtained at different times. An RV calibration function is fitted by using the fitted centers of the sky emission line, which can successfully calibrate the RV deviations of nebulae in real time. The future released value-added catalog of MRS-N will apply this RV calibration function to provide accurate RVs of nebula emission lines. We suggest other MRS-N users to implement our method to investigate and also improve the RV precision of nebula spectra in the future.

Acknowledgements This project is supported by the National Key R&D Program of China (Grant No. 2017YFA0402704) and the National Natural Science Foundation of China (Grant Nos. 11903048, 12090041, 12090040, 11833006, 12073051, 11733006, 11403061, U1531118, 11973060, U1631131 and 11873057), the NAOC Nebula Talents Program and the Key Research Program of Frontier Sciences, CAS (Grant No. QYZDY-SSW-SLH007). C.-H. Hsia acknowledges the supports from The Science and Technology Development Fund, Macau SAR (file No. 061/2017/A2 and 0007/2019/A) and Faculty Research Grants of the Macau University of Science and Technology (program No. FRG-19-004-SSI).

Guoshoujing Telescope (the Large Sky Area Multi-Object Fiber Spectroscopic Telescope, LAMOST) is a National Major Scientific Project built by the Chinese Academy of Sciences. Funding for the project has been provided by the National Development and Reform Commission. LAMOST is operated and managed by the National Astronomical Observatories, Chinese Academy of Sciences.

Appendix A:

References

Alvarez, C., & Hoare, M. G. 2005, A&A, 440, 569
Blair, W. P., Long, K. S., & Vancura, O. 1991, ApJ, 366, 484
Cavichia, O., Costa, R. D. D., Maciel, W. J., & Mollá, M. 2017, MNRAS, 468, 272
Chen, B. Q., Liu, X. W., Ren, J. J., et al. 2017, MNRAS, 472, 3924
Cui, X.-Q., Zhao, Y.-H., Chu, Y.-Q., et al. 2012, RAA (Research in Astronomy and Astrophysics), 12, 1197
Damiani, F., Bonito, R., Magrini, L., et al. 2016, A&A, 591, A74
Deng, L.-C., Newberg, H. J., Liu, C., et al. 2012, RAA (Research in Astronomy and Astrophysics), 12, 735
Esteban, C., García-Rojas, J., Arellano-Córdova, K. Z., & Méndez-Delgado, J. E. 2019, arXiv e-prints, arXiv:1905.10129
Fesen, R. A., Blair, W. P., & Kirshner, R. P. 1985, ApJ, 292, 29
Gerardy, C. L., & Fesen, R. A. 2007, MNRAS, 376, 929
Kopsacheili, M., Zezas, A., & Leonidaki, I. 2020, MNRAS, 491, 889
Kwitter, K. B., Lehman, E. M. M., Balick, B., & Henry, R. B. C. 2012, ApJ, 753, 12
Liu, C., Fu, J., Shi, J., et al. 2020, arXiv e-prints, arXiv:2005.07210
Liu, N., Fu, J.-N., Zong, W., et al. 2019, RAA (Research in Astronomy and Astrophysics), 19, 075
Luo, A. L., Zhang, H.-T., Zhao, Y.-H., et al. 2012, RAA (Research in Astronomy and Astrophysics), 12, 1243
Luo, A. L., Zhao, Y.-H., Zhao, G., et al. 2015, RAA (Research in Astronomy and Astrophysics), 15, 1095
Merrett, H. R., Merrifield, M. R., Douglas, N. G., et al. 2006, MNRAS, 369, 120
Osterbrock, D. E., & Ferland, G. J. 2006, Astrophysics of gaseous nebulae and active galactic nuclei
Osterbrock, D. E., Fulbright, J. P., Martel, A. R., et al. 1996, PASP, 108, 277
Rebassa-Mansergas, A., Gänsicke, B. T., Rodríguez-Gil, P., Schreiber, M. R., & Koester, D. 2007, MNRAS, 382, 1377
Rebassa-Mansergas, A., Ren, J. J., Parsons, S. G., et al. 2016, MNRAS, 458, 3808
Rebassa-Mansergas, A., Ren, J. J., Irawati, P., et al. 2017, MNRAS, 472, 4193

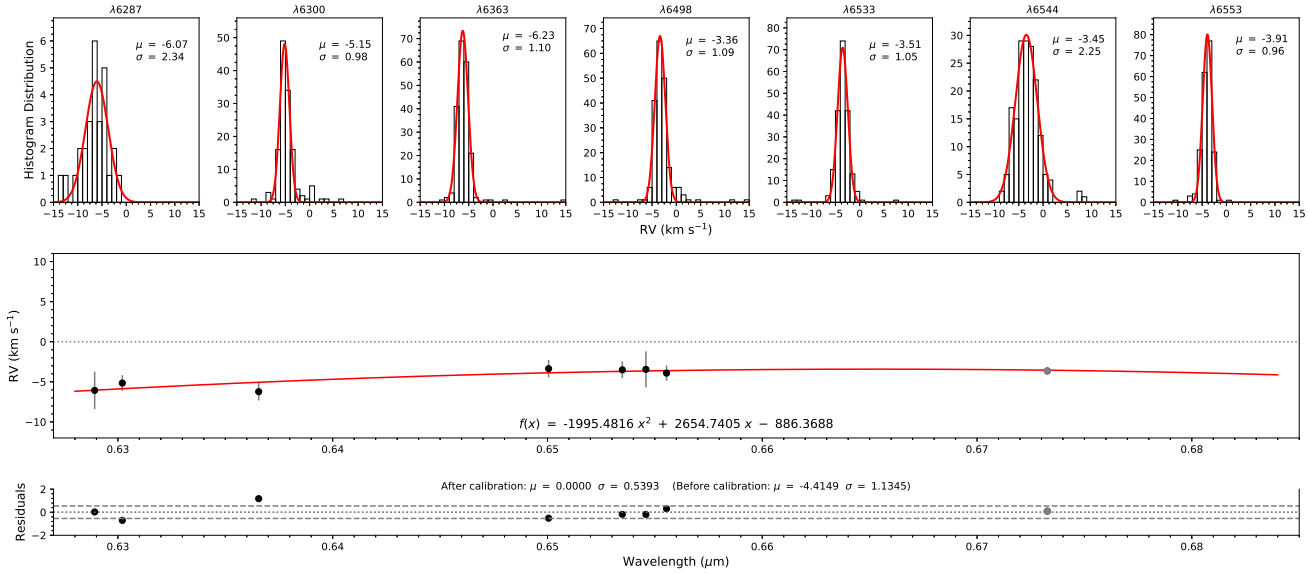

Fig. A.1 The *upper panels*: the histogram distribution of sky RVs for spectrograph ID 04 (i.e., "20180305-HD474690801-04"); *lower panels*: the corresponding fitted RV calibration function for this spectrograph.

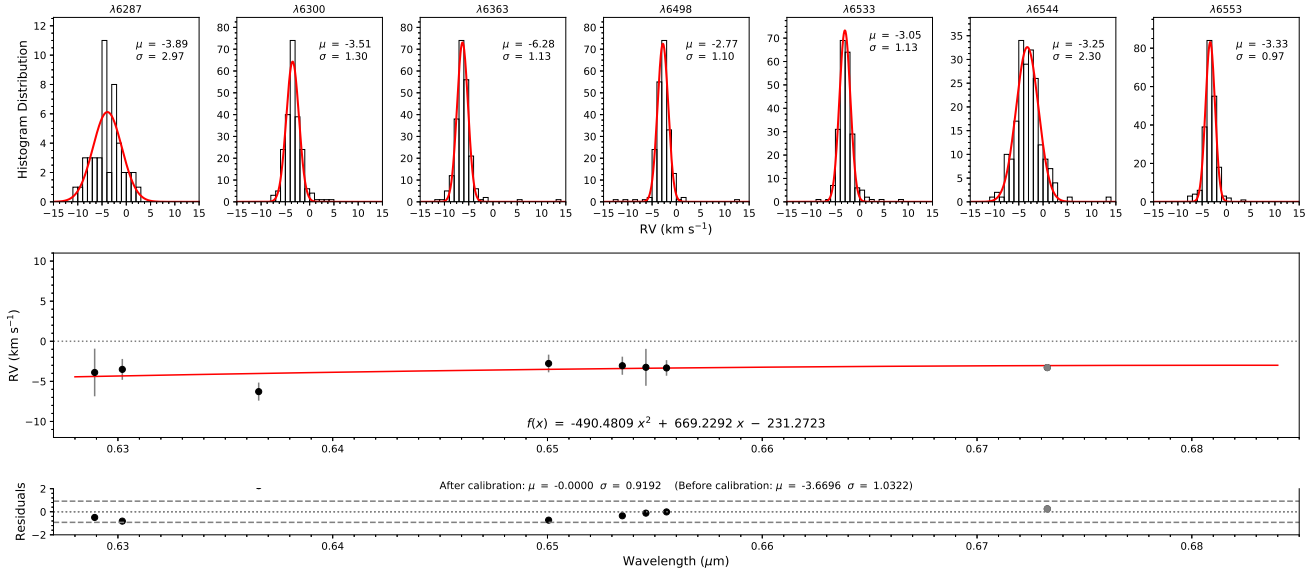

Fig. A.2 Same as Fig. A.1, but for spectrograph ID 08 (i.e., "20180305-HD474690801-08").

Ren, J. J., Rebassa-Mansergas, A., Parsons, S. G., et al. 2018a, MNRAS, 477, 4641

Ren, J. J., Rebassa-Mansergas, A., Luo, A. L., et al. 2014, A&A, 570, A107

Ren, J.-J., Liu, X.-W., Chen, B.-Q., et al. 2018b, RAA (Research in Astronomy and Astrophysics), 18, 111

Ren, J., Luo, A., Li, Y., et al. 2013, AJ, 146, 82

Shaver, P. A., McGee, R. X., Newton, L. M., Danks, A. C., & Pottasch, S. R. 1983, MNRAS, 204, 53

Su, D.-Q., & Cui, X.-Q. 2004, ChJAA (Chin. J. Astron. Astrophys.), 4, 1

Wang, R., Luo, A. L., Chen, J. J., et al. 2019, ApJS, 244, 27

Wang, S.-G., Su, D.-Q., Chu, Y.-Q., et al. 1996, Appl. Opt., 35, 5155

Woltjer, L. 1972, ARA&A, 10, 129

Wu, C.-J., Wu, H., Hsia, C.-H., et al. 2020a, RAA (Research in Astronomy and Astrophysics), 20, 033

Wu, C.-J., Wu, H., Zhang, W., et al. 2020b, arXiv e-prints, arXiv:2007.05240

Zhao, G., Zhao, Y.-H., Chu, Y.-Q., et al. 2012, RAA (Research in Astronomy and Astrophysics), 12, 723